Original Article

High-fat diet-induced obesity primes fatty acid β-oxidation impairment and consequent ovarian dysfunction during early pregnancy

Qingying Li[1,2], Sujuan Guo[1,2], Chengshun Yang[1,2], Xueqing Liu[1,2], Xuemei Chen[1,2], Junlin He[1,2], Chao Tong[3], Yubin Ding[1,2], Chuan Peng[4], Yanqing Geng[1,2], Xinyi Mu[1,2], Taihang Liu[1,2], Fangfang Li[1,2], Yingxiong Wang[1,2], Rufei Gao[1,2]

[1]Laboratory of Reproductive Biology, School of Public Health and Management, Chongqing Medical University, Chongqing, China; [2]Joint International Research Laboratory of Reproduction & Development, Chongqing Medical University, Chongqing, China; [3]Department of Obstetrics, The First Affiliated Hospital of Chongqing Medical University, Chongqing, China; [4]The Chongqing Key Laboratory of Translational Medicine in Major Metabolic Diseases, The First Affiliated Hospital of Chongqing Medical University, Chongqing, China

Contributions: (I) Conception and design: R Gao, Q Li; (II) Administrative support: C Yang; (III) Provision of study materials or patients: Q Li; (IV) Collection and assembly of data: Q Li, S Guo; (V) Data analysis and interpretation: Q Li; (VI) Manuscript writing: All authors; (VII) Final approval of manuscript: All authors.

Correspondence to: Yingxiong Wang; Rufei Gao. Laboratory of Reproductive Biology, School of Public Health and Management, Chongqing Medical University, Chongqing 400016, China; Joint International Research Laboratory of Reproduction & Development, Chongqing Medical University, Chongqing 400016, China. Email: yxwang@cqmu.edu.cn; gao_ru_fei@cqmu.edu.cn.

Background: Obesity is associated with many adverse effects on female fertility. Obese women have a higher likelihood of developing ovulatory dysfunction due to dysregulation of the hypothalamic-pituitary-ovarian axis. However, the effect of obesity on ovarian function during early pregnancy needs to be further assessed.

Methods: C57BL6/J mice were given a high-fat diet (HFD) for 12 weeks to induce obesity. An *in vitro* high-fat model was established by treating the human ovarian granulosa cell line KGN with oleic acid and palmitic acid. Ovarian morphology of obese mice in early pregnancy was assessed by hematoxylin and eosin staining and ovarian function was assessed by enzyme-linked immunosorbent assay, western blotting, and immunohistochemistry. Oil Red O staining and transmission electron microscopy were used to detect fatty acid accumulation. Specific markers relating to the ovarian functional mechanism were assessed by real-time PCR, western blotting, lactate detection, adenosine triphosphate (ATP) detection, biochemical analyses, and enzyme-linked immunosorbent assay.

Results: The results of this study showed that during early pregnancy, the number of corpus lutea, serum estradiol and progesterone levels, and the expression of the steroid biosynthesis-related protein CYP19A1 (aromatase), CYP11A1 (cholesterol side chain cleavage enzyme), and StAR (steroidogenic acute regulatory protein), were significantly increased in HFD mice. Mice fed an HFD also showed a significant increase in ovarian lipid accumulation on day 7 of pregnancy. Genes involved in fatty acid synthesis (*Acsl4* and *Elovl5*), and fatty acid uptake and transport (*Slc27a4*), together with the β-oxidation rate-limiting enzyme *Cpt1a*, were significantly upregulated in HFD mice. Specifically, there was abnormal elevation of ATP and aberrant expression of tricarboxylic acid cycle (TCA)- and electron transport chain (ETC)-related genes in the ovaries of pregnant HFD mice. KGN cells treated with etomoxir targeting β-oxidation of fatty acid showed decreased TCA cycle and ETC related gene expression. The elevation of ATP and estradiol and progesterone levels was reversed.

Conclusions: During early pregnancy, HFD-induced obesity increases fatty acid β-oxidation, which in turn increases TCA cycle and ETC related gene expression, leading to increased ATP production and ovarian dysfunction.

Keywords: Ovary; obesity; early pregnancy; fatty acid β-oxidation; glycolysis

Submitted Apr 10, 2021. Accepted for publication May 18, 2021.
doi: 10.21037/atm-21-2027
View this article at: http://dx.doi.org/10.21037/atm-21-2027

Introduction

Obesity is dramatically increasing in prevalence around the world. It has been reported to affect more than 650 million adults worldwide (1). Obesity describes an increase in body weight due to excessive accumulation of fatty tissue. The rise in obesity has in turn contributed to an increased prevalence of related metabolic dysfunction, cardiovascular diseases, diabetes, musculoskeletal disorders, and cancers (2). Furthermore, obesity exerts a negative impact on female fertility, and is associated with numerous adverse prenatal maternal and fetal effects (3). The rates of many pregnancy-related complications, such as hypertensive disorders, gestational diabetes, preterm birth, and other health challenges that warrant cesarean delivery, are higher in obese women than in women of a normal weight (3). However, the mechanisms underlying the adverse effects of obesity on female fertility have not been well elucidated.

The ovary is the female gonad and an important endocrine organ. The main functions of the ovary include the production, maturation, and release of oocytes, and the synthesis of female sex steroid and peptide hormones that regulate reproductive and non-reproductive functions (4). Environmental factors can exhaust the oocyte pool and induce the depletion of follicular cells, premature ovarian failure, early menopause, and infertility. Obese women are more likely than women of a normal weight to suffer ovulatory dysfunction due to dysregulation of the hypothalamic-pituitary-ovarian axis (5,6). However, the impact of obesity on ovarian functions during early pregnancy is unclear.

Approximately 15% of miscarriages occur during early pregnancy (7). During this time, female sex steroid hormones, particularly estrogen and/or progesterone, directly regulate the expression of several genes in the uterus to help maintain the pregnancy. Sufficient levels of estrogen and progesterone reduce the risk of miscarriage (7-9). The regulatory effect of estrogen and progesterone on the ovaries and the uterus during early pregnancy renders the endometrium more receptive to blastocysts by inducing endometrial secretory changes which are essential for successful implantation and decidualization. Therefore, investigation of the impact of obesity on ovarian functions would help to clarify the mechanistic basis of the association between obesity and female infertility.

Glucose and free fatty acids (FFAs) are the body's major energy sources (10). Also, mitochondrial β-oxidation of FFAs is a major avenue for adenosine triphosphate (ATP) production (11). Whenever the metabolism of glucose and FFAs are disturbed—due to an inappropriate diet, unhealthy lifestyle, or other factors—tissue and organ functions become dysregulated. In obese individuals, many tissues and organs, including skeletal muscle, are well known to exhibit dysregulation of glucose uptake, lipid metabolism, and mitochondrial function (12,13). However, whether ovarian glucose and fatty acid homeostasis are dysregulated by diet-induced obesity during early pregnancy has not been extensively investigated.

Therefore, in the present study, we investigated ovarian functions and assessed the integrity of ovarian glucose and fatty acid homeostasis during early pregnancy in mice with high-fat diet (HFD)-induced obesity. Our findings will provide theoretical bases for exploration of the effects and mechanisms of ovarian dysfunction in obese maternal mice during early pregnancy, and offer a scientific basis for a comprehensive evaluation of obesity as a risk factor for female infertility.

We present the following article in accordance with the ARRIVE reporting checklist (available at http://dx.doi.org/10.21037/atm-21-2027).

Methods

Animals

C57BL6/J mice (4 weeks old) were purchased from Charles River Laboratories, Beijing, China. The animals were housed in cages under a 12/12-hour light/dark cycle and an ambient temperature (22–25 ℃). After acclimation on an ordinary diet for 1 week, female mice were fed either a chow diet (Research Diets, D12450J) or a HFD (Research Diets, D12492) for 12 weeks. The chow diet consisted of 20%

protein, 10% fat, and 70% carbohydrates, while the HFD consisted of 20% protein, 60% fat, and 20% carbohydrates. The mice were weighed weekly. After 12 weeks, the female mice were mated with fertile males of the same strain, which were fed with normal diet. Day 1 of pregnancy (D1) was recorded as the day on which a vaginal plug appeared. On D7 of pregnancy, serum and tissue samples were collected and stored for further study. Experiments were performed under a project license (No. SCXK [YU] 2012-0001) granted by the Ethics Committee of Chongqing Medical University, in compliance with Chongqing Medical University guidelines for the care and use of animals.

Cell culture

The human ovarian granulosa cell line KGN was purchased from EK-Bioscience (Shanghai, China) and authenticated via short tandem repeat (STR) analysis by Cellcook Biotech (Guangzhou, China). The cells were cultured at 37 ℃ in Dulbecco's Modified Eagle Medium/F-12 medium (Gibco, USA) supplemented with 10% fetal bovine serum (Gibco, USA) and 1% penicillin-streptomycin (Beyotime, Shanghai, China). To establish a high-fat cell model, cells were treated with 400 μM oleic acid (OA, Sigma, USA) and 200 μM palmitic acid (PA, Sigma, USA) for 24 hours. After that, luteinization was induced in the cells through 12-hour treatment with 1IU human chorionic gonadotropin (hCG, Merck, Germany).

Real-time polymerase chain reaction

Total RNA was extracted from mouse ovarian tissues and KGN cells with Trizol reagent (Invitrogen, USA). Complementary DNA was synthesized using a PrimeScript™ RT reagent Kit with gDNA Eraser (TaKaRa, Dalian, China). Real-time reverse transcription-polymerase chain reaction (RT-PCR) was performed using GoTaq® qPCR Master Mix (Promega, USA) and the ABI ViiATM7 real-time fluorescence quantitative PCR system. Data were analyzed using the ΔΔCt method and were normalized to β-actin. Primer sequences are listed in *Tables 1* and *2*.

Western blot

Tissues and cells were homogenized in radioimmunoprecipitation assay (RIPA) buffer (Beyotime, Shanghai, China) with protease and phosphatase inhibitor cocktail (Thermo Fisher, USA). The protein concentration was measured using a bicinchonic acid (BCA) assay kit (Beyotime, Shanghai, China). Equal amounts of protein were separated by 10% sodium dodecyl sulphate–polyacrylamide gel electrophoresis (SDS-PAGE) and then transferred onto a polyvinylidene difluoride (PVDF) membrane. The nonspecific binding sites on the membranes were blocked with 5% non-fat milk at room temperature for 1 hour, after which, the membranes were incubated with primary antibodies (*Table 3*) at 4 ℃ overnight. After washing the membranes with phosphate-buffered saline with Tween, we incubated them with anti-rabbit or anti-mouse immunoglobulin G secondary antibody conjugated with horseradish peroxidase. Finally, an enhanced chemiluminescent (ECL) detection kit (Millipore, Germany) was employed to visualize the bands on the membranes. The light density and grey level were analyzed and calculated by using ImageJ (Bio-Rad, USA), with β-actin used as a loading control.

Biochemical analyses

Blood was centrifuged at 3,000 rotations per minute for 10 minutes under 4 ℃ to obtain the serum. The serum levels of triglyceride (TG) and total cholesterol (TC) were determined using specific assay kits (Nanjing Jiancheng, Nanjing, China) and applying glycerol-3-phosphate oxidase p-aminophenol (GPO-PAP) and cholesterol oxidase-peroxidase coupling (COD-PAP) methods. Homogenization of mouse ovarian tissue and KGN cells was carried out with absolute ethyl alcohol over ice. Then, the TG content was analyzed by applying the GPO-PAP method, following the protocol supplied with the triglyceride test kit (Nanjing Jiancheng, Nanjing, China). The TG levels in tissues and cells were expressed as mol/g protein. Protein concentration was detected using a BCA protein assay kit.

Enzyme-linked immunosorbent assay

Estradiol and progesterone levels in serum and cell medium were determined using commercial enzyme-linked immunosorbent assay kits (ELISA, Yanhui Biotech, Shanghai, China) following the manufacturer's protocol. Absorbance was read at 450 nm using a microplate reader (ThermoFisher Scientific, USA).

Hematoxylin and eosin staining

Ovarian tissues were fixed with 4% paraformaldehyde and

Table 1 Sequences of forward and reverse primers used for real-time reverse transcription-polymerase chain reaction (RT-PCR) of mouse ovarian tissues

Gene	Forward (5'→3')	Reverse (5'→3')
Slc2a1	CAGTTCGGCTATAACACTGGTG	GCCCCCGACAGAGAAGATG
Slc2a4	ATGGGCTTTCTCCGTCCTG	TTCAGTGGAAGTGCCAGTTTGT
Hk2	TGATCGCCTGCTTATTCACGG	AACCGCCTAGAAATCTCCAGA
Pfkl	TGCAGCCTACAATCTGCTCC	GTCAAGTGTGCGTAGTTCTGA
Pgk1	GGTCGTGATGAGGGTGGAC	CAGCAGAGATTTGAGTTCAGCA
Pkm2	CGCCTGGACATTGACTCTG	GAAATTCAGCCGAGCCACATT
Ldha	CAAAGACTACTGTGTAACTGCGA	TGGACTGTACTTGACAATGTTGG
Pdha1	TGTGACCTTCATCGGCTAGAA	TGATCCGCCTTTAGCTCCATC
Pdk1	GGACTTCGGGTCAGTGAATGC	TCCTGAGAAGATTGTCGGGGA
Acsl4	TCCTCCAAGTAGACCAACCCC	AGTCCAGGGATACGTTCACAC
Elovl5	CAGATCACCGTGCTCCATGTC	CTGTTGAGTGTCGCACCAAA
Cd36	GGAGCCATCTTTGAGCCTTCA	GAACCAAACTGAGGAATGGATCT
Slc27a4	ACTGTTCTCCAAGCTAGTGCT	GATGAAGACCCGGATGAAACG
Hadha	TGCATTTGCCGCAGCTTTAC	GTTGGCCCAGATTTCGTTCA
Cpt1a	TGGCATCATCACTGGTGTGTT	GTCTAGGGTCCGATTGATCTTTG
Cs	GGACAATTTTCCAACCAATCTGC	AGTCAATGGCTCCGATACTGC
Idh2	GGAGAAGCCGGTAGTGGAGAT	GGTCTGGTCACGGTTTGGAA
Suclg1	GGATACGACACGGGTCTTACA	GTGGTTCCTCCCACGAGTTTG
Sdh2	GGAACGGAGACAAGTACCTGG	TGGCAGCGGTAGACAGAGAA
Mdh2	TTGGGCAACCCCTTTCACTC	GCCTTTCACATTTGCTCTGGTC
Ndufb6	TGGAAGAACATGGTCTTTAAGGC	TTCGAGCTAACAATGGTGTATGG
Cox10	AGAAGAGCTATACAGGGATTGCC	CTGTGTGACATACATGCGCTT
Atp5b	GGTTCATCCTGCCAGAGACTA	AATCCCTCATCGAACTGGACG
β-actin	GGCTGTATTCCCCTCCATCG	CCAGTTGGTAACAATGCCATGT

embedded in paraffin. The embedded tissues were sectioned at 5-μm intervals and stained with hematoxylin and eosin (H&E), and the morphological changes in the HFD-fed mice were assessed.

Immunohistochemistry

Paraffin-embedded sections (5-μm in thickness) were deparaffinized and treated with citrate repair solution in a microwave oven for 5 minutes at high fire and 15 minutes at low fire. After repair, the rabbit Streptavidin Peroxidase (SP) kit (ZSGB-BIO, Beijing, China) was used for the subsequent immunohistochemical experiments. First, endogenous peroxidases in the tissues were inhibited via incubation with 3% hydrogen peroxide for 10 minutes at room temperature. After that, the nonspecific binding sites were blocked with 10% goat serum for 30 minutes at 37 ℃, which was followed by incubation with primary antibodies (*Table 3*) overnight at 4 ℃. Then, the sections were incubated with horseradish peroxidase-conjugated secondary antibody for 30 minutes at 37 ℃. Finally, peroxidase activity was detected using 3,3-diaminobenzidine substrate (DAB, ZSGB-BIO, Beijing, China). The sections were counterstained with hematoxylin. ImageJ was used for

Table 2 Sequences of forward and reverse primers used for real-time reverse transcription-polymerase chain reaction (RT-PCR) of human KGN cells

Gene	Forward (5'→3')	Reverse (5'→3')
SLC2A1	GGCCAAGAGTGTGCTAAAGAA	ACAGCGTTGATGCCAGACAG
PFK2	ATTGCGGTTTTCGATGCCAC	GCCACAACTGTAGGGTCGT
PGK1	TGGACGTTAAAGGGAAGCGG	GCTCATAAGGACTACCGACTTGG
LDHA	TTGACCTACGTGGCTTGGAAG	GGTAACGGAATCGGGCTGAAT
PDHA1	CACTGATTACTACAAGAGAGGCGATTT	CGGACGCACAGGATATCCAT
ACSL4	CATCCCTGGAGCAGATACTCT	TCACTTAGGATTTCCCTGGTCC
ELOVL5	AATCAGACACGGCACCTT	CACCCTACACCCTTCCTA
CD36	GGCTGTGACCGGAACTGTG	AGGTCTCCAACTGGCATTAGAA
SLC27A4	GTGAAGGCAAAGGTGCGAC	CGGAAGGTCCAGTGGGTATC
HADHA	ATATGCCGCAATTTTACAGGGT	ACCTGCAATAAAGCAGCCTGG
CPT1A	TCCAGTTGGCTTATCGTGGTG	TCCAGAGTCCGATTGATTTTTGC
CS	CTGGAGACTGGGTGAAAGTGACTAC	GGCCCCCTGAAACAAAAGTATACT
IDH2	TCAAGCTGAAGAAGATGTGGAAAA	AGACAGTCCCCCCCAGGAT
SUCLG1	ACATGGTACGAGTCAAGCACAAA	GGGCCCAATTAGCCTTGTC
SDH2	GACACCAACCTCAATAAGGTCTC	GGCTCAATGGATTTGTACTGTGC
MDH2	CCTTGTGGATGCAATGAATGG	GGTACATTCCGTTTCCTGTGACTT
NDUFB6	CCACAGAAGATGGGGCCTATG	TCCAGACAGGTACAAGTACATGA
COX10	CACCGCCCAGCCTATCTTTG	TCATCTCTTTCCACCGCTTTTC
ATP5B	AAACAATTTGCTCCCATTCATGC	GACAACCTTGATACCAGTCACC
β-actin	TAGTTGCGTTACACCCTTTCTTG	CACCTTCACCGTTCCAGTTTT

quantification of the positive area.

Transmission electron microscopy

Tissue specimens were fixed in 2.5% glutaraldehyde, dehydrated in graded alcohol, and stained with OsO4 and uranyl acetate. After that, the sections were polymerized and cut in preparation for examination under a Hitachi H-7650 transmission electron microscope (Hitachi, Japan).

Oil Red O staining

Ovarian tissues were fixed in 4% paraformaldehyde for 24 hours and then in 30% sucrose for 1 hour, after which they were embedded in optimal cutting temperature compound (OCT) and serially sectioned at 4 μm intervals. KGN cells were cultured on 13-mm round glass coverslips. After incubation in 60% isopropyl alcohol for 5 minutes, both the sections and cells were stained with freshly prepared 0.15% Oil Red O (Solarbio, Beijing, China) for 10 minutes. To remove unspecific attachments, the sections and cells were then washed in 60% isopropyl alcohol. Finally, the sections and cells were counterstained with hematoxylin and mounted with glycerol jelly.

Lactate detection

Mouse ovarian tissue was homogenized on ice and centrifuged at 12,000 g at 4 ℃ for 5 minutes, and the supernatant was taken for lactate detection. For KGN cells, the culture medium was directly used for lactate detection. A lactate test kit (Nanjing Jiancheng, Nanjing, China) was used to determine the lactate content according to the manufacturer's instructions. Briefly, 1 mL enzyme reagent,

Table 3 Antibodies used for western blotting and immunohistochemistry (IHC)

Peptide/protein target	Species	Manufacturer, catalog	The concentration of IHC	The concentration of Western Blotting
Aromatase (CYP19A1)	Rabbit	AB clonal, ab18995	1:200	1:1,000
Cytochrome P450 family 11 subfamily A member 1 (CYP11A1/P450Scc)	Rabbit	Boster, BA2120	1:100	1:500
Steroidogenic acute regulatory protein (StAR)	Rabbit	Bioss, bs-3570R	1:100	1:1,000
Hypoxia-inducible factor 1-alpha (HIF-1α)	Rabbit	AB clonal, A11945	1:100	1:1,000
Pyruvate dehydrogenase phosphatase1 (PDP1)	Rabbit	AB clonal, A6332	1:50	1:500
Phosphoinositide-dependent kinase1 (PDK1)	Rabbit	Boster, BA4499	1:100	1:1,000
Pyruvate dehydrogenase E1 alpha 1 (PDHA1)	Rabbit	AB clonal, A1895	1:500	1:5,000
Carnitine palmitoyltransferase 1A (CPT1A)	Rabbit	Proteintech, 15184-1-AP		1:1,000
β-Actin	Mouse	Boster, BM0005		1:1,000

and 0.2 mL color-substrate solution were added to the samples, mixed well, and incubated in a 37 ℃ water bath for 10 minutes. Then, 2 mL stop buffer was added, and finally, the absorbance was measured at 530 nm using a microplate reader (ThermoFisher Scientific, USA). The lactate content was normalized to the total protein content.

ATP detection

ATP levels were measured using an ATP assay kit (Beyotime, Shanghai, China). Tissues and cells were homogenized on ice, and centrifuged at 12,000 g at 4 ℃ for 5 minutes to obtain the supernatant. ATP detection reagent was added to the supernatant, and relative light unit (RLU) value was measured with a luminometer at 10 s RLU. The concentration was calculated based on an ATP standard curve and expressed as mol/mg. Protein concentration was determined using the BCA protein assay kit.

Cell Counting Kit-8 (CCK-8) assay

KGN cells were seeded on a 96-well microtiter plate (5.0×10^3 cells/well), and a Cell CCK-8 assay kit (Dojindo, Japan) was used to determine the number of viable cells. CCK-8 reagent was added to each well and incubated for 2 hours. Finally, the absorbance of each well was measured at 450 nm.

Statistical analysis

Differences between 2 groups were determined using unpaired Student's *t* test (2-tailed). Differences among 3 groups were calculated by 1-way analysis of variance (ANOVA), while differences within groups were assessed using the Mann-Whitney test. All data were expressed as mean ± standard error of the mean (SEM). All statistical analyses were performed with GraphPad Prism version 5.4 (GraphPad Software Inc., USA). Differences were considered significant when $P<0.05$. All experiments were repeated at least 3 times.

Results

HFD-induced obesity impairs ovarian function during early pregnancy

After a 12-week period on an HFD diet, female C57BL/6J mice showed increased body weight (*Figure 1A*,*B*). Compared with the controls, the HFD mice had significantly elevated fasting levels of circulating serum TG and TC (*Figure 1C*,*D*). Since embryo implantation and decidualization are related to the levels of estrogen and progesterone, which are produced by the corpus lutea of the ovary (14), we examined the effects of HFD-induced obesity on the ovaries of mice during early pregnancy. Assessment of the luteal structure on D7 by H&E staining showed a significant increase in the number of corpus lutea in the HFD group compared to CON group (*Figure 1E*,*F*). On D7, serum levels of estradiol and progesterone were measured to further explore the effect of HFD-induced obesity on luteal function. As shown in *Figure 1G*,*H*, HFD-induced obesity increased the serum estradiol and

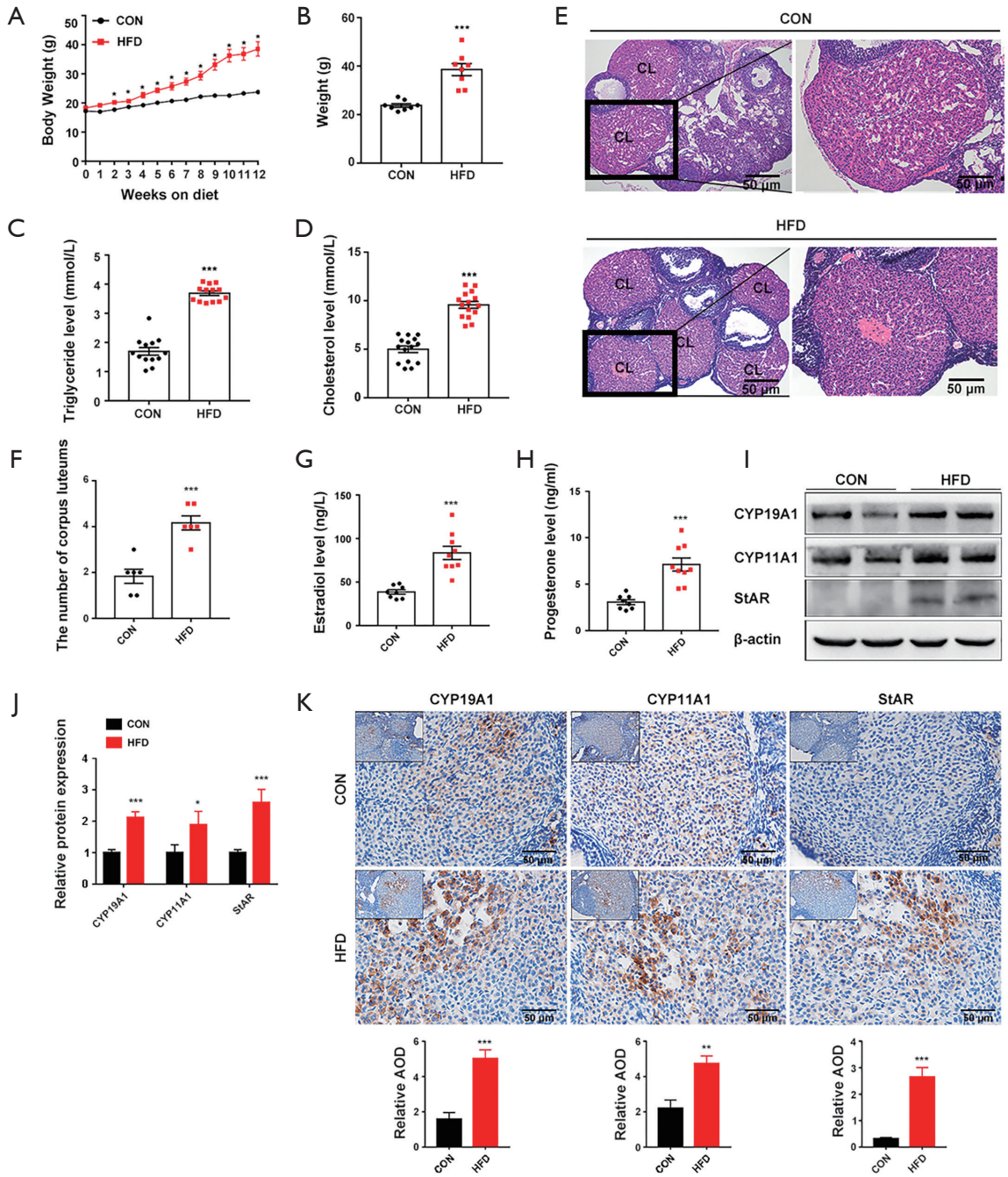

Figure 1 Mice with HFD-induced obesity exhibit aberrant ovarian function in early pregnancy. (A) Body weights of female mice fed either a chow diet or a HFD for 12 weeks. (B) Body weights of female mice on day 7 of pregnancy. Serum (C) triglyceride and (D) total cholesterol levels of mice fed a chow or HFD on day 7 of pregnancy. (E) Ovarian morphology was assessed by H&E staining on day 7 of pregnancy. (F) The number of corpus lutea in the control and HFD-treated groups. Serum (G) estradiol and (H) progesterone levels on day 7 of pregnancy were detected by ELISA. (I) Western blot results showing the ovarian protein expression of CYP19A1, CYP11A1, and StAR on day 7 of pregnancy. (J) Histogram showing the statistical analysis of western blot on E. (K) Immunolocalization results showing CYP19A1, CYP11A1, and StAR expression in the corpus lutea. AOD (IOD/area) was used for the quantitative analysis of immunohistochemical staining, and the data are shown in bar graphs. *P<0.05, **P<0.01 and ***P<0.001. CL, corpus luteum; CON, chow diet group; HFD, high-fat diet group; AOD, average optical density; IOD, integrated optical density.

progesterone levels considerably.

CYP19A1, CYP11A1, and steroidogenic acute regulator (StAR) are well known to be linked to the regulation of steroid biosynthesis. CYP19A1 is a cytochrome P450 enzyme that is responsible for the aromatization of testosterone into estradiol (15), while StAR and the cholesterol side-chain cleavage enzyme (P450scc), which is encoded by CYP11A1, catalyze the first and rate-limiting steps of steroid biosynthesis (16,17). On D7, we observed a significant increase in the expression of CYP19A1, CYP11A1, and StAR in the HFD-fed pregnant mice compared to the control group (*Figure 1I,J,K*). Taken together, our results indicated that ovarian function was impaired by HFD-induced obesity.

Ovarian glycolysis is not altered by HFD-induced obesity during early pregnancy

Hyperglycemia and dyslipidemia are 2 metabolic alterations of obesity, a condition which is associated with dysregulation of glucose and fatty acid metabolism in tissues and organs (18). To shed light on the possible mechanism by which HFD-induced obesity impairs ovarian function during early pregnancy, we first explored whether glycolysis, the central pathway of glucose metabolism (19), is affected by obesity. Results showed that the Slc2a1 (code glucose transporter 1 protein) and Slc2a4 (code glucose transporter 4 protein), as well as the key glycolytic enzymes hexokinase 2 (Hk2), pyruvate kinase M2 (Pkm2), and phosphoglycerate kinase 1 (Pgk1), were similarly expressed in the ovaries of pregnant mice in both the HFD group and the control group on D7 (*Figure 2A*). High expression of pyruvate dehydrogenase kinase 1 (PDK1) has previously been reported to reduce pyruvate dehydrogenase (PDH) activity by inducing the phosphorylation of its E1α subunit (PDHA1). Subsequently, energy metabolism shifts from oxidative phosphorylation to aerobic glycolysis (20). Furthermore, hypoxia-inducible factor-1 (HIF1) can transform cells from aerobic oxidation to anaerobic glycolysis through activation of the switch protein PDK1 (21). Our results revealed no significant difference in ovarian HIF1α, PDK1, PDP1, or PDHA1 expression between the HFD group and the control group on D7 (*Figure 2B,C,D,E*). This finding suggests that the impaired ovary exhibited no obvious energy metabolic shifts between aerobic and anaerobic glycolysis during early pregnancy. Moreover, there was an absence of significant changes in ovarian lactate production in the HFD group (*Figure 2F*), confirming that ovarian glycolysis was not significantly altered by HFD-induced obesity during early pregnancy.

HFD-induced obesity enhances fatty acid β-oxidation in the ovary during early pregnancy

Based on its availability, ATP can trigger different cell responses, including cell proliferation, differentiation, and apoptosis (22-24). In this study, the concentration of ATP in mouse ovarian tissue on D7 was significantly increased by HFD obesity (*Figure 3A*). Due to the stability of ovarian glycolysis in mice with HFD-induced obesity during early pregnancy, we speculated that the abnormally elevated ATP level in the dysfunctional ovary had mainly resulted from disordered fatty acid metabolism. Thus, we first examined the effect of HFD-induced obesity on lipid accumulation in the ovary. An HFD induced a significant increase in ovarian lipid accumulation, as evidenced by the quantitative results of lipid content, and Oil Red O staining and transmission electron microscopy of ovarian tissue from the mice on D7 (*Figure 3B,C,D*). Moreover, genes involved in fatty acid synthesis (*Acsl4* and *Elovl5*), and fatty acid uptake and transport (*Slc27a4*), together with the β-oxidation rate-limiting enzyme *Cpt1a*, were significantly upregulated in mice with HFD-induced obesity on D7 (*Figure 3E,F,G*). These observations suggest that HFD-induced obesity enhances fatty acid β-oxidation in the ovary during early pregnancy. Mitochondrial fatty acid β-oxidation, the ETC, and the tricarboxylic acid cycle (TCA) cycle are interrelated pathways involved in the eukaryotic cellular bioenergetics (25). Specifically, some genes involved in the TCA cycle and ETC were also found to be abnormally expressed in the ovaries of HFD pregnant mice on D7 (*Figure 3H*). Taken together, these results suggest that during early pregnancy, HFD-induced obesity primes fatty acid β-oxidation, which in turn increases gene expression related to TCA cycle and ETC, and consequently increases ATP production and ovarian dysfunction.

Fatty acid β-oxidation contributes to the impairment of ovarian function by HFD-induced obesity

PA (16:0) is the most abundant non-esterified fatty acid in the Western diet, and in the blood (26-28), and OA (18:1) is the most abundant monounsaturated non-esterified fatty acid in human serum (27,28). Cell loading with FFAs has been commonly used to construct *in vitro* models of obesity. In the present study, a mixture consisting of 400 μM OA

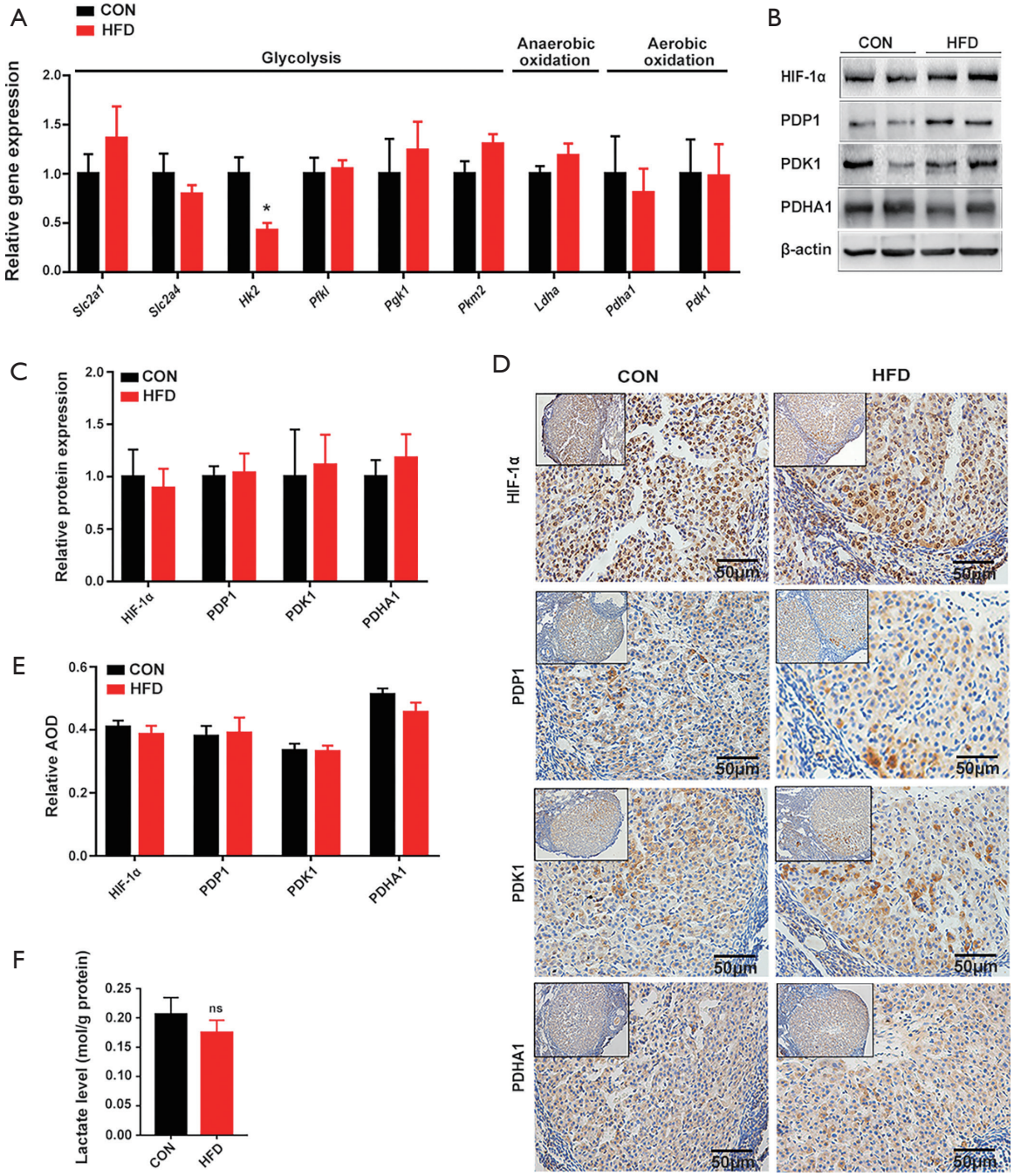

Figure 2 Ovarian glycolysis is not altered by HFD–induced obesity during early pregnancy. (A) Real-time PCR shows that key glycolysis-regulatory genes including *slc2a1*, *slc2a4*, *hk2*, *pkm2*, *pgk1*, *pfkl*, *ldha*, *pdha1* and *pdk1* are stably expressed in the ovaries of pregnant mice in the HFD group on D7. For each group, n=15. (B) Western blot analysis shows that the ovarian expression of proteins (HIF-1α, PDP1, PDK1, PDHA1) in the HFD group, these proteins play a role in shifting the energy metabolism between aerobic and anaerobic glycolysis, is comparable with that in the control group on D7. (C) Histogram showing the statistical analysis of western blot on B. Each group n=6. (D) According to immunohistochemistry, the expression and the location of proteins HIF1α, PDK1, PDH, and PDHA1 are not obviously altered on D7 in mice fed an HFD. (E) Histogram showing the statistical analysis of immunohistochemistry on D. (F) There is no significant change in ovarian lactate production in the HFD group compared with the control group on D7. Each group n=8–10. *P<0.05. CON, chow diet control group; HFD, high-fat diet group.

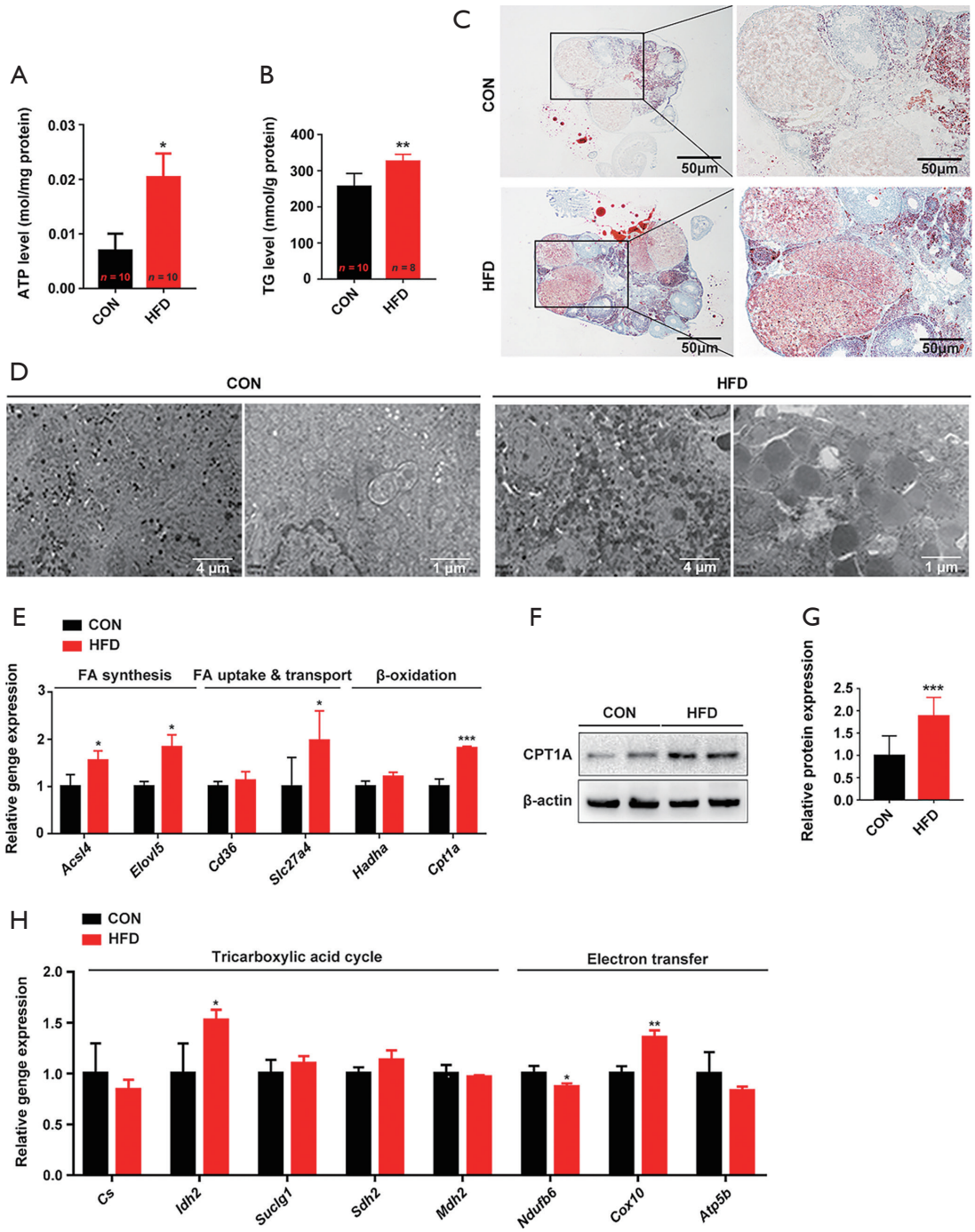

Figure 3 High-fat diet-induced obesity enhances fatty acid β-oxidation in the ovary during early pregnancy. Ovarian tissues on D7 of pregnancy were examined to examine the role of high-fat diet-induced obesity in fatty acid metabolism during early pregnancy. (A) ATP production in the ovarian tissues of pregnant mice on D7. According to the (B) quantitative results of lipid content, (C) Oil Red O staining, and (D) transmission electron microscopy image analysis, a high-fat diet causes a significant increase in ovarian lipid accumulation. (E) Genes involved in fatty acid metabolism were detected by real-time PCR. Each group n=15. (F) The fatty acid β-oxidation rate-limiting enzyme CPT1A was examined by western blot. (G) Histogram showing the statistical analysis of western blot on F. Each group n=6. (H) The expression of genes involved in the tricarboxylic acid cycle and electron transport chain were detected by real-time PCR. *P<0.05, **P<0.01, and ***P<0.001.

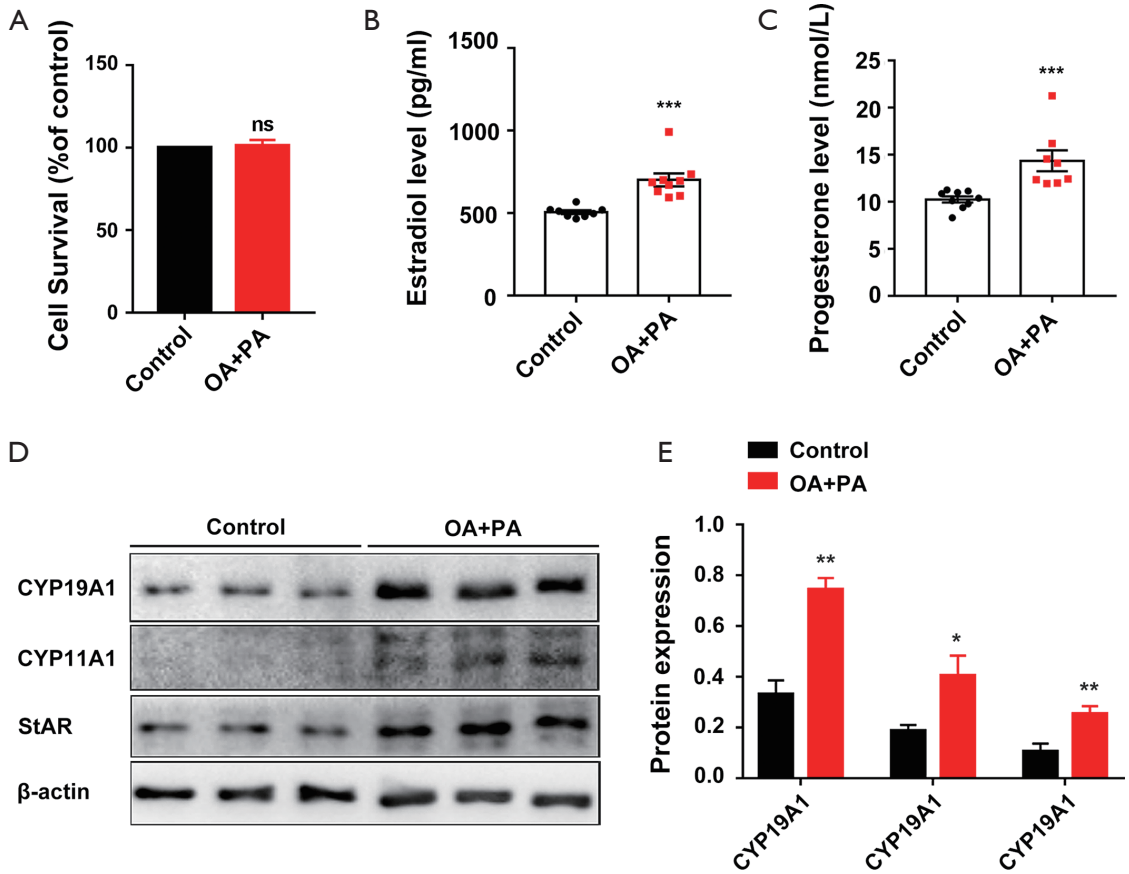

Figure 4 Palmitic acid and oleic acid induced ovarian dysfunction in luteinized KGN cells. Luteinized KGN cells were treated with a mixture of 400 μM OA and 200 μM PA (OA/PA, 2:1) for 24 hours. (A) Cell viability. Each group n=5. Exocellular estradiol (B) and progesterone (C) levels are significantly increased in OA- and PA-treated KGN cells. Each group n=8–9. (D) The expression of steroid biosynthesis genes, including of CYP19A1, CYP11A1 and StAR, was detected by western blot. Each group n=6. (E) Histogram showing the statistical analysis of western blot on D. *P<0.05, **P<0.01, and ***P<0.001. OA, oleic acid; PA, palmitic acid.

and 200 μM PA was used at a non-cytotoxic concentration to further probe the role of HFD-induced obesity in compromised ovarian function during early pregnancy *in vitro* (*Figure 4A*). We found that the levels of exocellular estradiol and progesterone were significantly increased in OA- and PA-treated KGN cells (*Figure 4B,C*). Exposure to OA and PA significantly increased the protein expressions of genes that regulate steroid biosynthesis, including CYP19A1, CYP11A1, and StAR, in luteinized KGN cells (*Figure 4D,E*).

Consistent with the *in vivo* results, neither lactate production nor the expression of glycolysis-regulating factors in OA and PA-treated KGN cells showed a significant change (*Figure 5*). These results suggest that the glycolysis of luteinized KGN cells is not obviously altered by treatment with OA and PA *in vitro*. Given our earlier observation of ATP elevation and stable glycolysis, we hypothesized that the abnormally increased levels of ATP in dysfunctional KGN cells also mainly resulted from dysfunctional fatty acid β-oxidation. According to the results, lipid droplet accumulation and intracellular TG content were both significantly increased in OA and PA-treated KGN cells (*Figure 6A,B,C*). We further detected the ATP concentration in KGN cells, and the results showed that the levels of ATP were significantly increased following OA and PA treatment (*Figure 6D*). Moreover, the β-oxidation rate-limiting enzyme CPT1A was also dramatically upregulated by OA and PA treatment in KGN cells compared to the control group (*Figure 6E,F*).

Etomoxir is a widely used small molecule that is capable

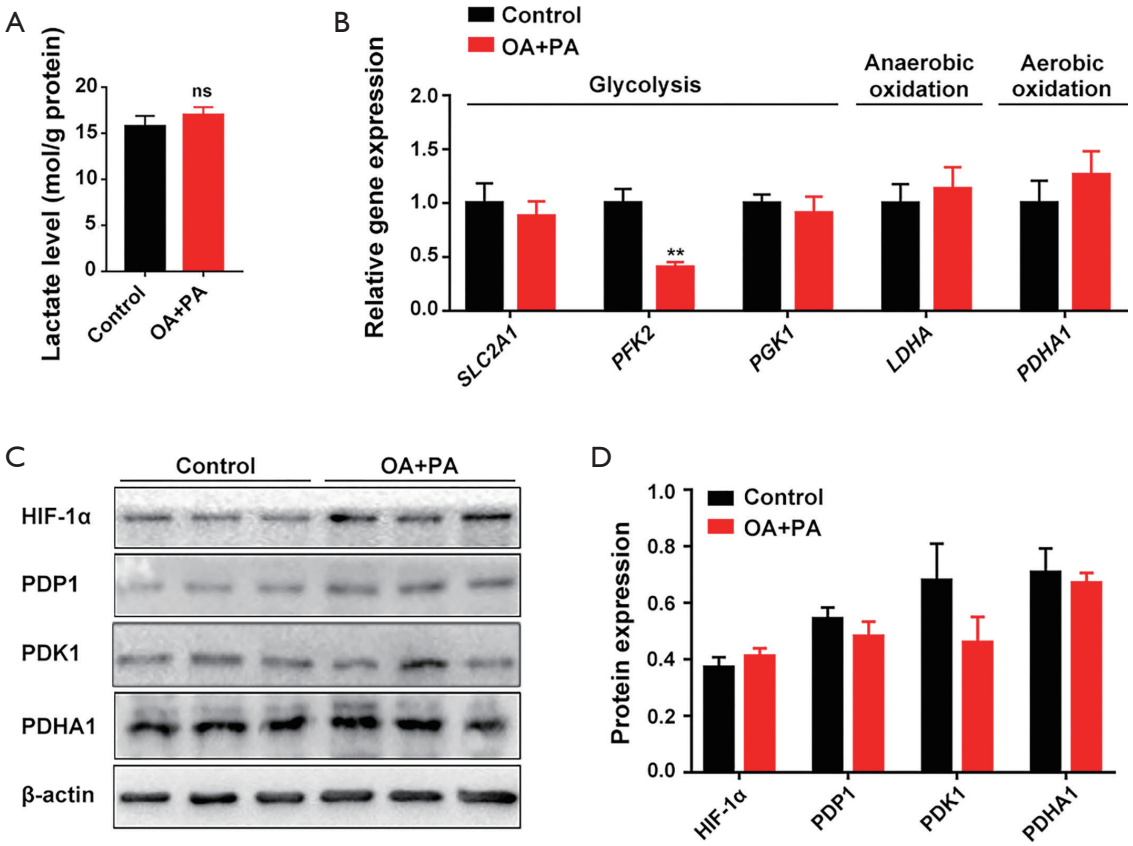

Figure 5 Glycolysis in luteinized KGN cells was not apparently altered by palmitic acid and oleic acid. (A) Lactate production. (B) Real-time PCR results show that the key genes regulating glycolysis including *SLC2A1*, *PGK1*, *PFK2*, *LDHA* and *PDHA1* are stably expressed in luteinized KGN cells treated with palmitic acid and oleic acid. (C) Western blot results show that the expression levels of HIF1α, PDK1, PDP1, and PDHA1 are not apparently altered by palmitic acid and oleic acid. (D) Histogram showing the statistical analysis of western blot on C. **P<0.01. OA, oleic acid; PA, palmitic acid.

of fatty acid oxidation inhibition, which it achieves by exerting an irreversible inhibitory effect on CPT1A (29). Following interference of β-oxidation of fatty acid with 100 μM etomoxir, the compromise of the TCA cycle and ETC, and the elevation of ATP by OA and PA were also reversed (*Figure 6G,H*). Etomoxir treatment further reversed the HFD-induced dysfunctional state of the KGN cells, as indicated by a significant decrease in the exocellular estradiol and progesterone levels compared with those in cells treated with OA and PA alone (*Figure 6I,J*). Steroid biosynthesis regulatory genes (CYP19A1, CYP11A1, and StAR) were also downregulated (*Figure 6K,L*).

Discussion

Obesity has been reported to carry an increased risk of complications in pregnancy, including miscarriage (3). However, the related underlying mechanisms have not been well elucidated. In early pregnancy, competent blastocysts adhere to the decidualized endometrium to invade the uterine tissue and vessels and to establish the pregnancy. During this time, estrogen and progesterone are secreted by the corpus lutea of the ovaries (30,31), so as to ensure the success of decidualization. Women with obesity are more likely to experience ovulatory dysfunction due to dysregulation of the hypothalamic-pituitary-ovarian axis (3). However, the ovarian functionality of women with obesity during early pregnancy is still unclear.

In this study, we used an HFD to induce obesity in maternal mice and then assessed their ovarian function. According to our results, HFD-fed female mice showed increased numbers of corpus lutea and elevated serum

estradiol and progesterone levels during early pregnancy. Significantly increased exocellular estradiol and progesterone levels were also found in luteinized KGN cells following treatment with OA and PA. All of these *in vivo* and *in vitro* results indicate that HFD-induced obesity impairs ovarian function during early pregnancy.

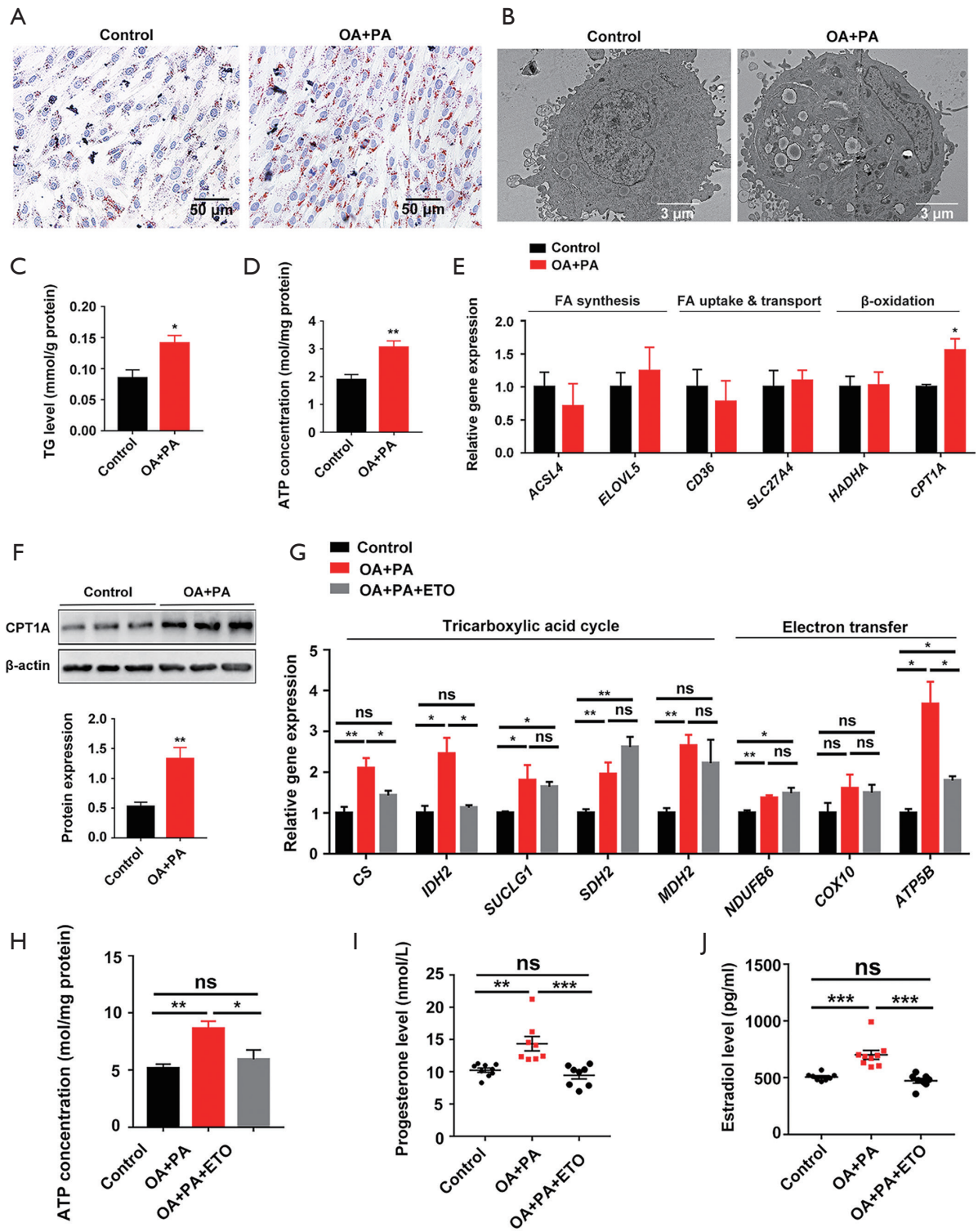

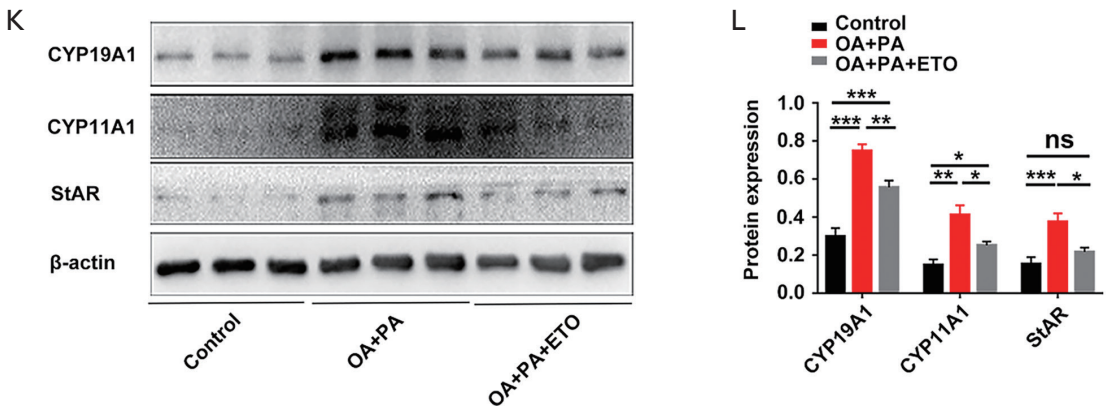

Figure 6 Fatty acid β-oxidation contributes to impaired ovarian function in luteinized KGN cells treated with palmitic acid and oleic acid. The accumulation of lipid droplets in KGN cells was examined by (A) Oil Red O staining and (B) transmission electron microscopy. Each group n=5. (C) Intracellular TG content is significantly increased in OA- and PA-treated KGN cells. Each group n=8. (D) The ATP concentration in KGN cells treated with PA and OA. Each group n=8. (E) Real-time PCR and (F) western blot results show that the expression of CPT1A in KGN cells is dramatically upregulated by PA and OA. Each group n=10. (G) The compromise of the tricarboxylic acid cycle and electron transport chain, and (H) the elevation of ATP by PA and OA are reversed by ETO. Each group n=8. After treatment with ETO, exocellular (I) estradiol and (J) progesterone levels are significantly decreased compared to those in cells treated with PA and OA alone. Each group n=7–8. (K,L) The expression of steroid biosynthesis genes, including of CYP19A1, CYP11A1, and StAR, is dramatically downregulated by ETO. Each group n=6. *P<0.05, **P<0.01, ***P<0.001. OA, oleic acid; PA, palmitic acid; ETO, etomoxir.

Obesity has been found to be associated with dysregulation of glucose and fatty acid metabolism in tissues and organs, including adipose tissue, the liver, muscle, the pancreas, and the brain (32,33). To understand the mechanisms by which HFD-induced obesity impairs ovarian function during early pregnancy, we first sought to establish whether impaired glycolysis is involved. According to our *in vivo* and *in vitro* results, ovarian glycolysis is not altered by HFD-induced obesity. Also, the impaired ovaries exhibited no obvious energy metabolic shifts between aerobic and anaerobic glycolysis.

Approximately 90–95% of ATP production comes from oxidative phosphorylation of mitochondria, and glycolysis accounts for the rest. Mitochondrial fatty acid oxidation is the main source of ATP in many tissues and organs (34). Fatty acid oxidation is a complex biological process involving mitochondrial β-oxidation, TCA cycle activity, and the ETC (35). Alterations in fatty acid metabolism can contribute to a variety of pathologies and cell dysfunction (36). Mitochondrial fatty acid oxidation is the main source of ATP in many tissues and organs (34,37). The maintenance of lipid homeostasis is a highly complex process involving lipid storage, synthesis, and utilization. During obesity, when the levels of FFAs exceed the lipid storage capacity of the adipose tissue, FFAs begin to accumulate in the organs. This condition—known as "ectopic lipid deposition"—has several pathologic consequences (38).

Given our earlier observation of the stability of glycolysis, we hypothesized that ovarian dysfunction mainly results from disordered fatty acid metabolism. When an HFD was used to induce obesity in the mice, we found that lipid droplets accumulated in the ovary during early pregnancy. The TG levels in the ovary were also elevated. These data indicate that ectopic lipid deposition in the ovary is involved in HFD-induced obesity. To identify the lipid metabolism-associated genes whose ovarian expressions are altered following the induction of obesity, we tested several genes involved in fatty acid synthesis, transportation and β-oxidation.

The results showed that ovarian *Acsl4* and *Elovl5* (which are involved fatty acid synthesis) and *Slc27a4* (which is involved in fatty acid transportation) were dramatically upregulated in obese mice during early pregnancy. CPT1A is the rate-limiting enzyme that transfers the long-chain fatty acyl-CoA to the mitochondria for β-oxidation (39). Upregulation of this enzyme was also observed in the obese mice. The upregulated expression of CPT1A *in vivo* and *in vitro* suggests that HFD-induced obesity primes an aberrant increase in fatty acid β-oxidation in the ovary during early pregnancy. Etomoxir is widely used as a potent

irreversible CPT1A inhibitor (40). In this study, when etomoxir was used to interfere with β-oxidation of fatty acid, lipid droplet accumulation and the levels of exocellular estradiol and progesterone levels in OA- and PA-treated KGN cells were improved. All of these results suggest that HFD-induced obesity enhances fatty acid β-oxidation in the ovaries of mice during early pregnancy.

ATP is the direct energy source for all kinds of life activities. Depending on its decrease or increase, ATP can trigger multiple different cell responses, including cell proliferation, differentiation and apoptosis (18,22-24). In the present study, the concentration of ATP in ovarian tissue during early pregnancy was significantly increased by HFD-induced obesity. Consistent with our *in vivo* results, ATP levels were found to be significantly increased in OA- and PA-treated KGN cells. Mitochondria meet the energy demands of cells via the uptake and oxidation of various substrates. This leads to the generation of acetyl CoA to produce ATP via TCA cycle oxidation (41). The transfer of electrons via the mitochondrial co-factors NAD(H) and FAD(H2) to the ETC creates a proton gradient across the inner mitochondrial membrane generating the mitochondrial membrane potential (41). This drives oxidative phosphorylation, which generates ATP via the reduction of oxygen to water and the phosphorylation of ADP (41). In the current study, we found that some genes involved in the TCA cycle and ETC were also abnormally expressed in the ovaries of obese pregnant mice. The compromise of the TCA cycle and ETC, and the elevation of ATP in OA- and PA-treated KGN cells were reversed following treatment with etomoxir. All of these observations suggest that during early pregnancy, HFD-induced obesity can prime fatty acid β-oxidation impairment, which in turn compromises the TCA cycle and ETC, consequently increasing ATP production and ovarian dysfunction.

In conclusion, our findings indicate that ovarian functions are impaired by HFD-induced obesity during early pregnancy in mice. Abnormal fatty acid β-oxidation, but not abnormal glycolysis, contributes to the impairment of ovarian functions in HFD-induced obesity. Our findings help in understanding the mechanistic effect of obesity on the ovaries and female fertility, and reinforces the need to regulate fat intake so as to avoid obesity and its associated effects. However, confirmation of our findings in humans is still needed.

Acknowledgments

Funding: This work was supported by the National Key Research and Development Program of China (grant no. 2018YFC1004401), the Science and Technology Research Program of Chongqing Municipal Education Commission (grant no. KJQN201900413), and the Natural Science Foundation of Chongqing (grant number cstc2020jcyj-msxmX0041).

Footnote

Reporting Checklist: The authors have completed the ARRIVE reporting checklist. Available at http://dx.doi.org/10.21037/atm-21-2027

Data Sharing Statement: Available at http://dx.doi.org/10.21037/atm-21-2027

Conflicts of Interest: All authors have completed the ICMJE uniform disclosure form (available at Available at http://dx.doi.org/10.21037/atm-21-2027). The authors have no conflicts of interest to declare.

Ethical Statement: The authors are accountable for all aspects of the work in ensuring that questions related to the accuracy or integrity of any part of the work are appropriately investigated and resolved. Experiments were performed under a project license (No. SCXK [YU] 2012-0001) granted by the Ethics Committee of Chongqing Medical University, in compliance with Chongqing Medical University guidelines for the care and use of animals.

References

1. Obesity and overweight. World Health Organization. 2020. Available online: https://www.who.int/news-room/fact-sheets/detail/obesity-and-overweight. Accessed 2021/03/01 2021.
2. Barathikannan K, Chelliah R, Rubab M, et al. Gut Microbiome Modulation Based on Probiotic Application

for Anti-Obesity: A Review on Efficacy and Validation. Microorganisms 2019;7:456.
3. Broughton DE, Moley KH. Obesity and female infertility: potential mediators of obesity's impact. Fertil Steril 2017;107:840-7.
4. Ding N, Harlow SD, Randolph JF Jr, et al. Perfluoroalkyl and polyfluoroalkyl substances (PFAS) and their effects on the ovary. Human Reproduction Update 2020;26:724-52.
5. Pasquali R, Pelusi C, Genghini S, et al. Obesity and reproductive disorders in women. Hum Reprod Update 2003;9:359-72.
6. Practice Committee of tAmerican Society for Reproductive Medicine. Definitions of infertility and recurrent pregnancy loss. Fertil Steril 2008;90:S60.
7. Ye Q, Cai S, Wang S, et al. Maternal short and medium chain fatty acids supply during early pregnancy improves embryo survival through enhancing progesterone synthesis in rats. J Nutr Biochem 2019;69:98-107.
8. El-Zibdeh MY. Dydrogesterone in the reduction of recurrent spontaneous abortion. J Steroid Biochem Mol Biol 2005;97:431-4.
9. Duan L, Yan D, Zeng W, et al. Effect of progesterone treatment due to threatened abortion in early pregnancy for obstetric and perinatal outcomes. Early Human Development 2010;86:41-3.
10. Melkonian EA, Schury MP. Biochemistry, Anaerobic Glycolysis. StatPearls. Treasure Island (FL), 2020.
11. Stremmel W, Pohl L, Ring A, et al. A new concept of cellular uptake and intracellular trafficking of long-chain fatty acids. Lipids 2001;36:981-9.
12. Gabriel BM, Zierath JR. Circadian rhythms and exercise - re-setting the clock in metabolic disease. Nature reviews Endocrinology 2019;15:197-206.
13. Cervera IP, Gabriel BM, Aldiss P, et al. The phospholipase A2 family's role in metabolic diseases: Focus on skeletal muscle. Physiol Rep 2021;9:e14662.
14. Liu M, Deng T, He J, et al. Exposure to Benzo[a]pyrene impairs the corpus luteum vascular network in rats during early pregnancy. Environ Pollut 2020;259:113915.
15. Shimodaira M, Nakayama T, Sato I, et al. Estrogen synthesis genes CYP19A1, HSD3B1, and HSD3B2 in hypertensive disorders of pregnancy. Endocrine 2012;42:700-7.
16. Hu MC, Hsu HJ, Guo IC, et al. Function of Cyp11a1 in animal models. Mol Cell Endocrinol 2004;215:95-100.
17. Terry K, McGrath M, Lee IM, et al. Genetic variation in CYP11A1 and StAR in relation to endometrial cancer risk. Gynecol Oncol 2010;117:255-9.
18. Wang JD, Chen WY, Li JR, et al. Aspirin Mitigated Tumor Growth in Obese Mice Involving Metabolic Inhibition. Cells 2020;9:569.
19. Mulukutla BC, Yongky A, Le T, et al. Regulation of Glucose Metabolism – A Perspective From Cell Bioprocessing. Trends Biotechnol 2016;34:638-51.
20. Kwak CH, Jin L, Han JH, et al. Ilimaquinone Induces the Apoptotic Cell Death of Cancer Cells by Reducing Pyruvate Dehydrogenase Kinase 1 Activity. Int J Mol Sci 2020;21:6021.
21. Li X, Li Y, Bai S, et al. NR2F1-AS1/miR-140/HK2 Axis Regulates Hypoxia-Induced Glycolysis and Migration in Hepatocellular Carcinoma. Cancer Manag Res 2021;13:427-37.
22. Nicotera P, Leist M, Ferrando-May E. Intracellular ATP, a switch in the decision between apoptosis and necrosis. Toxicol Lett 1998;102-103:139-42.
23. Atlante A, Giannattasio S, Bobba A, et al. An increase in the ATP levels occurs in cerebellar granule cells en route to apoptosis in which ATP derives from both oxidative phosphorylation and anaerobic glycolysis. Biochim Biophys Acta 2005;1708:50-62.
24. White N, Burnstock G. P2 receptors and cancer. Trends Pharmacol Sci 2006;27:211-7.
25. Wang Y, Palmfeldt J, Gregersen N, et al. Mitochondrial fatty acid oxidation and the electron transport chain comprise a multifunctional mitochondrial protein complex. J Biol Chem 2019;294:12380-91.
26. Ricchi M, Odoardi MR, Carulli L, et al. Differential effect of oleic and palmitic acid on lipid accumulation and apoptosis in cultured hepatocytes. J Gastroenterol Hepatol 2009;24:830-40.
27. Lopez-de-Andrés A, Jiménez-Trujillo M, Hernández-Barrera V, et al. Trends in the Prevalence of Depression in Hospitalized Patients with Type 2 Diabetes in Spain: Analysis of Hospital Discharge Data from 2001 to 2011. Plos One 2015;10:e0117346.
28. Yousif MD, Calder MD, Du JT, et al. Oleic Acid Counters Impaired Blastocyst Development Induced by Palmitic Acid During Mouse Preimplantation Development: Understanding Obesity-Related Declines in Fertility. Reprod Sci 2020;27:2038-51.
29. O'Connor RS, Guo L, Ghassemi S, et al. The CPT1a inhibitor, etomoxir induces severe oxidative stress at commonly used concentrations. Sci Rep 2018;8:6289.
30. Huet-Hudson YM, Andrews GK, Dey SK. Cell type-specific localization of c-myc protein in the mouse uterus: modulation by steroid hormones and analysis of the

periimplantation period. Endocrinology 1989;125:1683-90.
31. Massimiani M, Lacconi V, Civita FL, et al. Molecular Signaling Regulating Endometrium–Blastocyst Crosstalk. Int J Mol Sci 2019;21:23.
32. Mao Z, Zhang W. Role of mTOR in Glucose and Lipid Metabolism. Int J Mol Sci 2018;19:2043.
33. Watt MJ, Miotto PM, De Nardo W, et al. The Liver as an Endocrine Organ-Linking NAFLD and Insulin Resistance. Endocr Rev 2019;40:1367-93.
34. Hou T, Ma H, Wang H, et al. Sevoflurane preconditioning attenuates hypoxia/reoxygenation injury of H9c2 cardiomyocytes by activation of the HIF-1/PDK-1 pathway. PeerJ 2020;8:e10603.
35. Jin Y, Shen Y, Su X, et al. The Small GTPases Rab27b Regulates Mitochondrial Fatty Acid Oxidative Metabolism of Cardiac Mesenchymal Stem Cells. Front Cell Dev Biol 2020;8:209.
36. Yufeng C, Lu J, Yunhong L, et al. Bamboo-shaving polysaccharide protects against high-diet induced obesity and modulates the gut microbiota of mice. J Funct Foods 2018;49:20-31.
37. Alice S, Matthew MK. Mitochondrial Fatty Acid Oxidation Disorders Associated with Short-Chain Enoyl-CoA Hydratase (ECHS1) Deficiency. Cells 2018;7:46.
38. Nishi H, Higashihara T, Inagi R. Lipotoxicity in Kidney, Heart, and Skeletal Muscle Dysfunction. Nutrients 2019;11:1664.
39. Ruderman NB, Saha AK, Kraegen EW. Minireview: malonyl CoA, AMP-activated protein kinase, and adiposity. Endocrinology 2003;144:5166-71.
40. Schlaepfer I, Rider L, Rodrigues L, et al. Lipid Catabolism via CPT1 as a Therapeutic Target for Prostate Cancer. Molecular Cancer Therapeutics 2014;13:2361-71.
41. Bradley J, Swann K. Mitochondria and lipid metabolism in mammalian oocytes and early embryos. Int J Dev Biol 2019;63:93-103.

(English Language Editor: J. Reynolds)

Cite this article as: Li Q, Guo S, Yang C, Liu X, Chen X, He J, Tong C, Ding Y, Peng C, Geng Y, Mu X, Liu T, Li F, Wang Y, Gao R. High-fat diet-induced obesity primes fatty acid β-oxidation impairment and consequent ovarian dysfunction during early pregnancy. Ann Transl Med 2021;9(10):887. doi: 10.21037/atm-21-2027

